Mechanical phase inversion of Pickering emulsions via metastable wetting of rough colloids

Michele Zanini,[†, §,‡] Alberto Cingolani,[⊥,‡] Chiao-Peng Hsu,[†] Miguel Angel Fernandez Rodriguez,[†] Giuseppe Soligno,[#] Anna Beltzung,[⊥] Stefano Caimi,[⊥] Denise Mitrano,[#] Giuseppe Storti[⊥] and Lucio Isa[†]*

† Laboratory for Interfaces, Soft Matter and Assembly, Department of Materials, ETH Zürich, Zürich (Switzerland)

§ Van 't Hoff Laboratory for Physical and Colloid Chemistry, Debye Institute for Nanomaterials Science, Utrecht University, Utrecht (The Netherlands)

Condensed Matter and Interfaces, Debye Institute for Nanomaterials Science, Utrecht University, Utrecht (The Netherlands)

⊥ Department of Chemistry and Applied Biosciences, Institute for chemical and bioengineering, ETH Zürich, Zürich (Switzerland)

Process Engineering Department, Eawag, Swiss Federal Institute of Aquatic Science and Technology (Switzerland)

KEYWORDS: Rough colloids, Pickering emulsions, Emulsion phase inversion.

ABSTRACT: The possibility to invert emulsions from oil-in-water to water-in-oil (or vice versa) in a closed system, i.e. without any formulation change, remains an open fundamental challenge with many opportunities for industrial applications. We exploit particle surface roughness to induce wetting hysteresis and obtain mechanically-responsive Pickering emulsions. The phase inversion is solely caused by an in-situ switch of the particle wettability from metastable positions at the interface following the input of controlled mechanical energy. Oil-in-water emulsions can be prepared at low energy using mildly hydrophobic rough colloids, which are dispersed in water and weakly pinned at the interface, and switched to water-in-oil emulsions by a second emulsification at higher energy, which triggers the relaxation of the particle contact angle. The same principle is demonstrated for the complementary emulsions using mildly hydrophilic colloids initially dispersed in oil. Our route uniquely relies on the delicate interplay between particle surface design during synthesis and the energy of the emulsification process to encode a kinetic pathway for the phase inversion. Both organic and inorganic nanoparticles can be used, allowing for the future implementation of our strategy in a broad range of smart industrial formulations.

Colloidal particles and liquid interfaces bear significant importance in addressing fundamental scientific questions and present many opportunities in industrial applications, ranging from food [1] to heavy oil processing [2, 3]. Since the seminal observations of Ramsden and Pickering [4, 5], partially wetting colloidal particles trapped at liquid interfaces have been proposed as excellent emulsion and foam stabilizers. Depending on their wettability, particles larger than a few nanometers can have energies binding them to a fluid interface that easily exceed thermal energy by several orders of magnitude [6, 7]. Such trapping can thus provide kinetic stabilization, effectively arresting coalescence and phase separation of emulsions[8, 9, 10] and foams[11, 12].

In particle-stabilized emulsions, analogously to surfactants, the particle contact angle θ plays a fundamental role in defining the emulsion type [13, 14, 15]. In fact, hydrophobic ($\theta > 90°$) particles have the tendency to stabilize water droplets in oil (w/o), while hydrophilic colloids ($\theta < 90°$) preferentially form oil-in-water emulsions (o/w). Thus, canonically, two kinds of particles are required to stabilize the two types of emulsions. This scheme can be challenged by using more complex particles, i.e. with shape, chemical functionality and surface texture deviating from uniform, smooth and rigid spherical colloids [16, 17]. The huge development in the fabrication of patchy [18, 19, 20], non- spherical [21, 22] and unconventional particles, i.e. presenting tunable surface functionalization [23], morphology [24, 25, 26, 27] and architecture [28, 29], provides ample opportunities for new stabilization strategies.

Surface roughness and its tailoring have in particular emerged as a powerful tool to control emulsion-stabilization processes [30, 31, 32]. The key design concept is that, akin to macroscopic surfaces [33], surface roughness may induce large contact angle hysteresis at the single-particle level, i.e. a significant difference in the particle contact angle when adsorbing from the oil phase (advancing contact angle) or when adsorbing from water (receding contact angle). If the hysteresis is large enough, rough colloids can be made into “universal stabilizers”, namely particles that can stabilize both w/o and o/w emulsions depending exclusively on the phase from

which they breach the interface [32, 34]. This concept only works if the contact line is strongly pinned and thermally-driven relaxations towards equilibrium are prevented [35, 36, 37, 38, 39]. It has for instance been shown that a sufficient number of spherical-cap asperities in the >10nm range can lead to pinning energies greatly exceeding k_BT [32, 40]. Finally, the colloid size generally affects the size of the emulsified droplets [16].

Emulsion inversion, that is the switching of emulsion type from o/w to w/o or vice versa, can be achieved via different approaches. It can for instance be obtained by varying the water-to-oil ratio [41] (catastrophic inversion) or by tuning the particle contact angle [42] (transitional phase inversion). The latter can be triggered by variations of temperature [43], surfactant concentration [14, 44], pH and ionic strength [45, 46, 47, 48] , via ex-situ drying processes [49, 50] or by changing the kind of apolar phase [51]. Analogous arguments also proved to be valid for foams [52].

Nevertheless, all of these routes typically require a change in the formulation during emulsification and cannot take place in a closed system once the first kind of emulsion has been created. Rare exceptions report the switch from w/o to o/w emulsions by either varying the particle concentration in the apolar phase [53] or the mixing time [54]. In these studies, partially hydrophobized, aggregated fumed silica were used. At high particle concentrations or short emulsification times, w/o emulsions were observed; conversely, o/w emulsions were obtained for low solid loading and longer mixing. The authors suggested that the fumed silica particles in oil consisted of flocs, which used up silanol groups to build the interparticle bonds, resulting in clusters that were effectively more hydrophobic than single particles. In this case, emulsion inversion was possible via a collective mechanism involving multi-particle aggregates, which formed weaker structures at low solid loading and broke up over longer mixing time. The possibility to invert emulsions in a closed system by the design and control of single-particle properties remains an experimentally untapped possibility, previously theoretically proposed [15].

By tailoring particle surface roughness and adsorption kinetic pathways, we herein propose a general strategy to obtain stimulus-responsive Pickering emulsions able to undergo phase

inversion upon the externally triggered mechanical relaxation of the stabilizers' contact angle. The strategy is represented in Scheme 1. We start by synthesizing colloidal particles with controlled surface roughness and surface chemistry so that they have a mild preferential wetting for one of the two fluids, i.e. water or oil, but they may also be dispersed in the other one, i.e. oil or water, respectively. In particular, we disperse inorganic, (mildly) hydrophilic rough colloids in oil and organic, (mildly) hydrophobic rough colloids in water. Upon a first emulsification step, using low mechanical energy, w/o and o/w emulsions are found in the two cases, respectively. This result stems from contact-line pinning and trapping of the rough colloids in metastable positions at the interface. Here, the mechanical input of the emulsification process is not strong enough to allow the de-pinning and relaxation of the contact line over the particle surface in order to move toward their thermodynamic equilibrium position (corresponding to o/w emulsions for the organic, hydrophobic rough colloids initially dispersed in water and w/o emulsions for the inorganic, hydrophilic rough colloids initially suspended in oil, respectively). This step follows the existing design principle for "universal stabilizers" [32, 40] . Uniquely, in this work the full relaxation of the contact line can be induced by a second emulsification step at higher energy. In this case, the energy input is large enough to transport the rough particles through the interface, allowing them to relax from their initial metastable positions toward equilibrium. Given the corresponding change of wettability from effectively (kinetically) hydrophilic to thermodynamically hydrophobic (and vice versa), this causes an inversion of the local curvature of the droplets, leading to a mechanical phase inversion of the emulsion [15]. The whole process can be performed in a closed system, i.e. without altering the system's composition or adding any extra component. The inversion stems only from the control of the particle metastability at the interface, which is encoded a priori in the surface design during the synthesis; particles need to have surfaces heterogeneous enough to pin the contact line during gentle emulsification, but which additionally allow for relaxation upon stronger mechanical agitation. In this way, roughness becomes a dynamic tool to control emulsion stability.

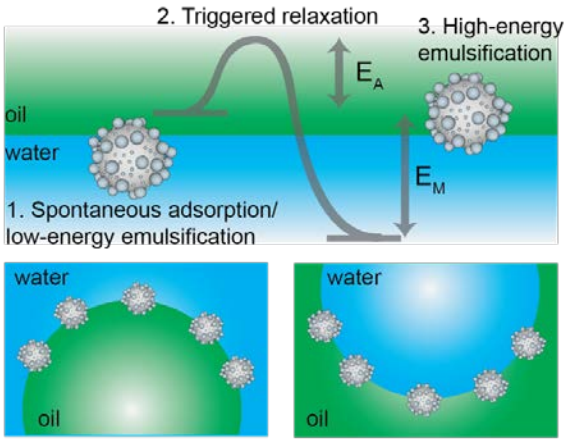

Figure 1 Mechanical phase inversion of Pickering emulsions. The scheme presents the process for the mechanical phase inversion of Pickering emulsions stabilized by metastable wetting of rough colloids. In particular, it is depicted the case of the inversion from o/w to w/o emulsions using mildly hydrophobic rough particles initially dispersed in water. The same line of thinking can be applied to the switching from w/o to o/w emulsions using mildly hydrophilic rough particles dispersed in oil before emulsification.

To demonstrate the general validity of our idea, we present hereafter two complementary sets of experiments. First, we synthesized organic, rough and moderately hydrophobic particles, which we dispersed in water and emulsified with equal amounts of n-decane to obtain o/w emulsions at low shear and water droplets in oil at higher emulsification energies. In complementary experiments, we synthesized inorganic, rough and mildly hydrophilic colloids, which we dispersed in n-decane (oil phase) and emulsified with equal amounts of water to obtain w/o emulsions at low input energies and o/w droplets at higher shear. The experiments are finally correlated to numerical simulations showing the free-energy trajectory of adsorbing colloids, which clearly highlights the presence of roughness-dependent metastable minima, underpinning the proposed mechanism for the mechanical inversion of the emulsions.

Results

Particle fabrication.

Our organic particles (D = 68±4 and 120±10 nm) present a core-shell architecture with a styrene-divinylbenzene (Sty-DVB) copolymer in the outer layer. The latter is directly and continuously

grown on different seeds (cores) via semi-batch emulsion polymerization [25, 55, 56] (Figure 2A and B). According to the desired final surface morphology, we adopted two strategies, both involving a direct switch from the core mixture feed to the shell one. In the case of standard smooth particles, hereon termed PS-I, the core already consists of poly(styrene-co-divinylbenzene) and the addition of the St-DVB monomer only results in a particle size increase without altering the morphology nor the composition (Figure 2A, Table S1 in the Supplementary Information). In the case of rough particles (PS-II), the core instead consists of poly(acrylonitrile) and the addition of the second feed containing St-DVB causes a phase separation during growth, due to the poor compatibility of the two polymeric matrices in the blend (no compositional gradient, Figure 2, synthesis path I). This phase separation in turns leads to the emergence of organic and rough surfaces [25, 56, 57]. The so-produced particles are hereon termed PS-II. For both PS-I and PS-II particles, the shell growth is carried out in so-called starved conditions, where the monomers are fed to the reaction vessel at a flow rate much smaller than their consumption rate by reaction, thus ensuring the production of a copolymer with instantaneous composition equal to that of the fed monomer mixture [58]. In this way, the control of the particle architecture (core/shell) and composition becomes straightforward [28, 29, 59]. Moreover, since Sty and DVB are the only monomers added during the shell growth, a chemically uniform polystyrene-based surface is ensured for both sets of particles. The same concept can also be used to produce particles with a smoother surface (see Figure 2B, synthesis path II, Table S2, Table S3, Figure S1 in the Supplementary Information), when the feed is gradually changed (moderate compositional gradient) and a slower core-to-shell transition is imposed. In this case, even though tuning the compositional gradient between core and shell growth enables a finer control over the roughness, it inevitably implies a heterogenous chemical composition of the particle's surface. For this reason, we later limit our emulsification studies to the PS-I and PS-II particles, which are compositionally analogous and thus allow isolating the effects of roughness. They have a moderately hydrophobic surface and are charge-stabilized in aqueous suspensions (ξ ~ -30 mV)

(see Supplementary Figure S2, Supplementary Section S1 and S3 in the Supplementary Information). Emulsification experiments on the other particle batches are presented in the Supporting Information, together with their surface morphology characterization (Figure S5 and Supplementary Section S2 in the Supplementary Information).

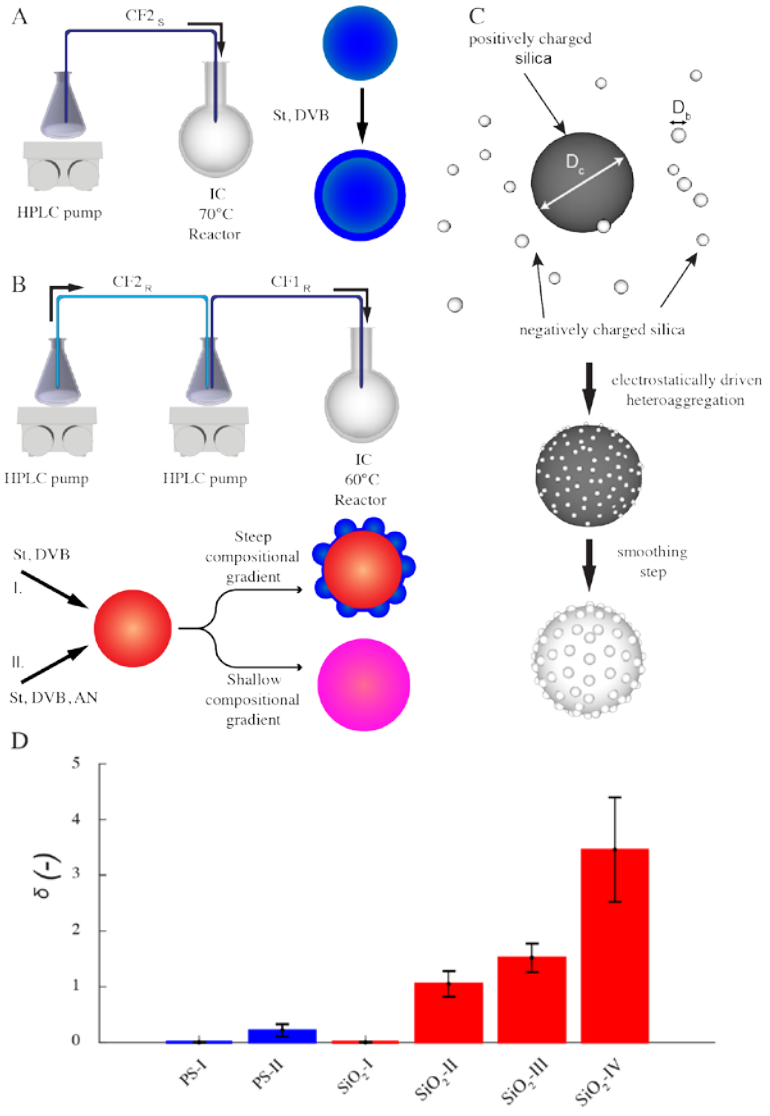

Figure 2 Synthesis of organic and inorganic rough colloids. (A) Synthesis scheme of organic homo-polymer core-shell smooth particles through two-step semibatch emulsion polymerization **(B)** Synthesis scheme of organic composite rough particles through two-step semibatch emulsion polymerization and phase separation; different feeds (I, II) lead to various morphologies and surface compositions. **(C)** Preparation of all-silica raspberry-like rough colloids via electrostatically driven heteroaggregation followed by surface smoothing. **(D)** Surface roughness of the various rough colloids expressed in terms of the

dimensionless parameter δ for the organic (blue) and inorganic (red) particles. The data are obtained from single-particle AFM analysis over at least 20 particles. Each bar represents the mean value and the error bars indicate the standard deviation extracted from the data distributions.

The inorganic rough colloids are instead all-silica raspberry-like particles (Figure 2C). They are fabricated by the electrostatically driven heteroaggregation of negatively charged silica nanoparticles (D_b = 22 ± 2 or 39 ± 4 nm) onto larger silica colloids (D_c = 161 ± 15, 374 ± 14 nm and 588 ± 21 nm), whose surface is rendered positively charged via polyelectrolyte adsorption. This initial step is followed by the controlled heteronucleation of silica layers (smoothing layer) on the raspberry-like particle surface via a sol-gel route [24, 32]. The surface roughness can be finely controlled by selecting the core-to-nanoparticles size ratio and by adjusting the thickness of the smoothing layer (~10 nm). Notably, the asperity lateral dimensions and height can be independently tailored through these two parameters. The as-produced hydrophilic all-silica raspberry-like particles are then partially hydrophobized using a uniform coating of bromo-silane to obtain a close-to-neutrally wetting surface, which makes them dispersible in both polar and apolar fluids [32, 60]. See the Methods Section and Supplementary Information Table S4 and Figure S3 for more details on the synthesis procedure.

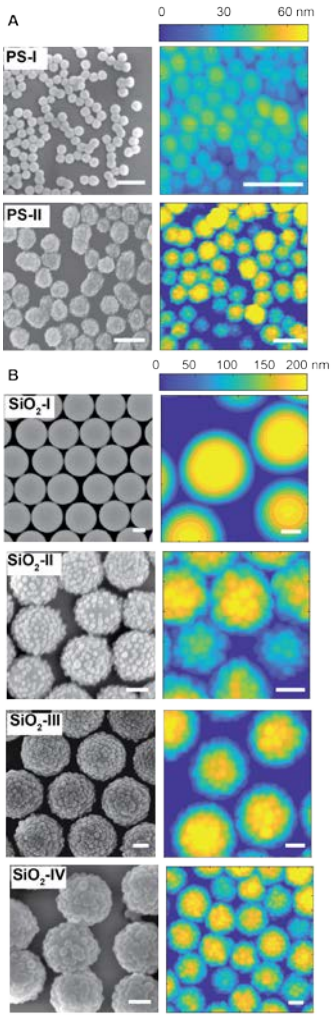

Figure 3 Topographical particle surface characterization. SEM and AFM surface analysis of the organic **(A)** and inorganic **(B)** rough colloids. Scale bars: 200 nm.

As reported in Figure 3A and B, the particles' surface topography is imaged and characterized by both scanning electron microscopy (SEM) and atomic force microscopy (AFM). Hereon, we describe the surface roughness with the dimensionless parameter $\delta = \frac{H}{d^2}R$, where *H* is the average asperity height, *d* the mean asperity-to-asperity distance and *R* the particle radius. In this way, provided that the asperities have comparable shapes, it is possible to differentiate the wetting behavior of colloids having different sizes of the core but decorated with features presenting the same roughness amplitude. The *δ* parameter directly describes the combined effect of number and size of asperities met by the moving three-phase contact line as the particle

crosses the fluid interface. *H/d* in fact represents an average roughness scale, while *R/d* is directly proportional to the linear density of asperities along the contact line. These two quantities are necessary to estimate a characteristic pinning force/energy [61], which we also use in our calculations (Table S5 and Supplementary Section S4 in the Supplementary Information). In the Supporting Information (Section S2 and Figure S4), we provide a direct comparison of the aforementioned roughness characterization with standard procedures and operators. The proposed fabrication methods allow synthesizing both organic and inorganic particles with roughness ~ $0 < \delta < 4$, irrespective from their composition.

Single-particle contact angle upon spontaneous adsorption.

After the synthesis and characterization, we measure the particle wettability as a function of surface roughness by means of a freeze-fracture shadow-casting technique coupled with cryo-SEM (FreSCa cryo-SEM) [62, 63]. Hereafter, particles adsorbing from the polar and apolar phase will be labeled with "w" and "o", respectively. Particles spontaneously adsorbing at a flat water/n-decane interface from either the aqueous or the oil phase are immobilized by shock-freezing. After removal of the frozen oil, tungsten is deposited on the vitrified aqueous phase with a well-defined tilt angle (30°) in high-vacuum and cryo conditions. Analogously to a sundial, particles protruding through the interface can cast a shadow. By measuring the shadow length and knowing the particle geometry, we extract their contact angle with single-particle resolution (see Figure 4). Smooth bromo-modified silica colloids adsorbing from n-decane (SiO_2-I_O) show a contact angle of ~ 70°, which coincides with their equilibrium position at the interface [32]. Rougher particles modified in the same fashion, which also spontaneously adsorb from the apolar phase (SiO_2-II_O, SiO_2-III_O and SiO_2-IV_O), display increasing contact angle values, becoming effectively hydrophobic in spite of their mildly hydrophilic surface chemistry. This trend confirms previous observations for larger colloids decorated with larger asperities and bearing the same surface functionality [32]. A mirrored behavior is observed for the organic rough particles adsorbing from water. The smooth PS reference (PS-I_w) reaches its equilibrium value of $\theta \approx 105°$ (see Figure 4) , but the rougher

colloids bearing the same surface chemistry (PS-II_W) become effectively hydrophilic due to trapping in metastable positions. The relation between the width of the contact angle distribution and the spread between the expected and the mean measured contact angle for rough colloids is reported in the Figure S11 in the Supplementary Information. The measured contact angle does not spontaneously evolve over times up to 10000 s (see Supplementary information Figure S6),suggesting that contact line relaxation for our rough colloids cannot proceed upon thermally activated hopping events [35].

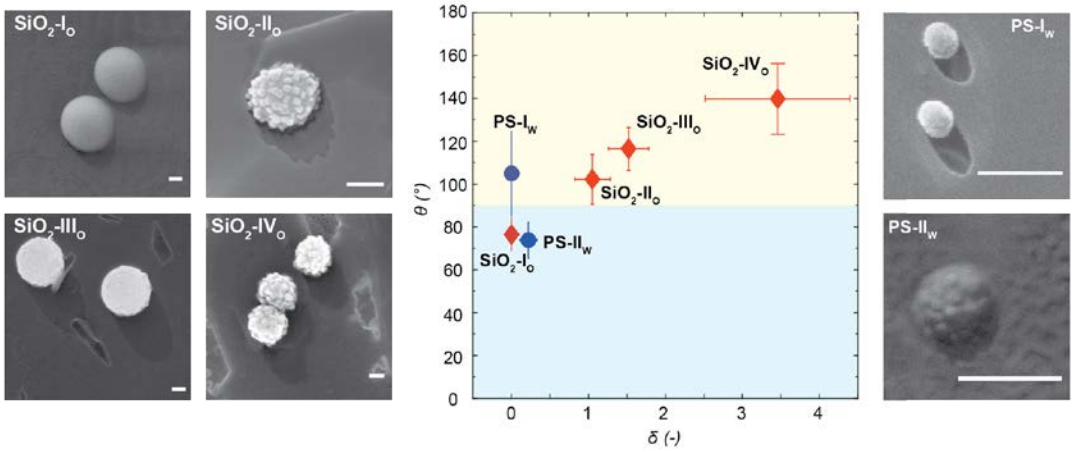

Figure 4 Particle contact angle upon spontaneous adsorption. Measured contact angles as a function of particle's surface roughness from FreSCa cryo-SEM images at a water/n-decane interface. The red diamonds represent the bromo-modified silica colloids spontaneously adsorbing from the oil phase. The blue dots depict the organic beads spontaneously adsorbing from the aqueous phase. Each point represents the mean value and the error bars indicate for the standard deviation extracted from the data distributions. The subscripts following the particle name indicate the phase, in which the particles are initially dispersed. Particles are immobilized shortly after adsorption (< 1 minute). Scale bars: 200 nm.

Mechanical phase inversion of Pickering emulsions.

In analogy to the Bancroft rule, as we will discuss later [9, 15, 64], (effectively) hydrophobic particles, such as PS-I_O, SiO_2-II_O, SiO_2-III_O and SiO_2-IV_O should give rise to w/o emulsions, while (effectively) hydrophilic particles, such as SiO_2-I_O and PS-II_W, to o/w emulsions. We show here that, for rough colloids trapped in metastable positions, this may or may not be true depending on

the energy input during emulsification. We start by emulsifying 1:1 water-to-oil mixtures in the presence of our colloids initially dispersed in either water or oil. We choose 1:1 mixtures to avoid any compositional bias to determine the emulsion type. As reported in Figure 5A-C, PS-I_W can only stabilize water-in-oil emulsions irrespective of the emulsification method. The emulsion type is confirmed by the macroscopic appearance of the emulsion and by conductivity measurements. The latter yield to zero and is not reported. Conversely, PS-II_W produces o/w emulsions when mixed at low energies (4000 rpm - Figure 5D or at 12000 rpm for < 1minute – Figure 5E) and the opposite emulsion when mixed at high shear rates (≥12000 rpm) for periods longer than 1 minute or if directly ultra-sonicated (Figure 5F). Interestingly, a short (≤ 1min) and intense emulsification step at high shear rates (≥12000 rpm) generates a dispersed phase but it is not yet sufficient to induce phase inversion (Figure 5E). In this case, conductimetry measurements are not feasible, due to the scarce thickness of the emulsion layer, but they are expected to match the conductivity of the continuous aqueous phase. Both fluorescence imaging in a drop test and conductivity experiments confirm the phase switch. In the drop test emulsions were diluted in an excess of the respective continuous phase, previously labelled with a fluorescent dye. In particular, we labeled water with a hydrophilic dye (Alexa Fluor 488 dye or Rhodamine B isothiocyanate) and n-decane with a hydrophobic one (Nile red or BODIPY 493/503). Therefore, in the drop test, o/w emulsions show dark oil droplets in a fluorescently labeled water background (Figure 5H), while w/o emulsions display dark water droplets dispersed in fluorescent oil (Figure 5I).The non-sphericity observed for some droplets suggests the presence of a viscoelastic interface [12, 65]. While the results obtained for PS-I_W confirm Bancroft-type predictions based on the wetting data from the FreSCa analysis, emulsions stabilized with PS-II_W follow the route proposed at the beginning of this manuscript. Notably, the mechanical switch can be triggered in-situ, i.e. the same the o/w emulsion produced at low shear rates can be inverted by a subsequent high-shear mixing or by ultra-sonication. As expected, mixtures with higher solid contents can stabilize larger volumes of the dispersed phase (see Figure S7 in Supplementary Information).

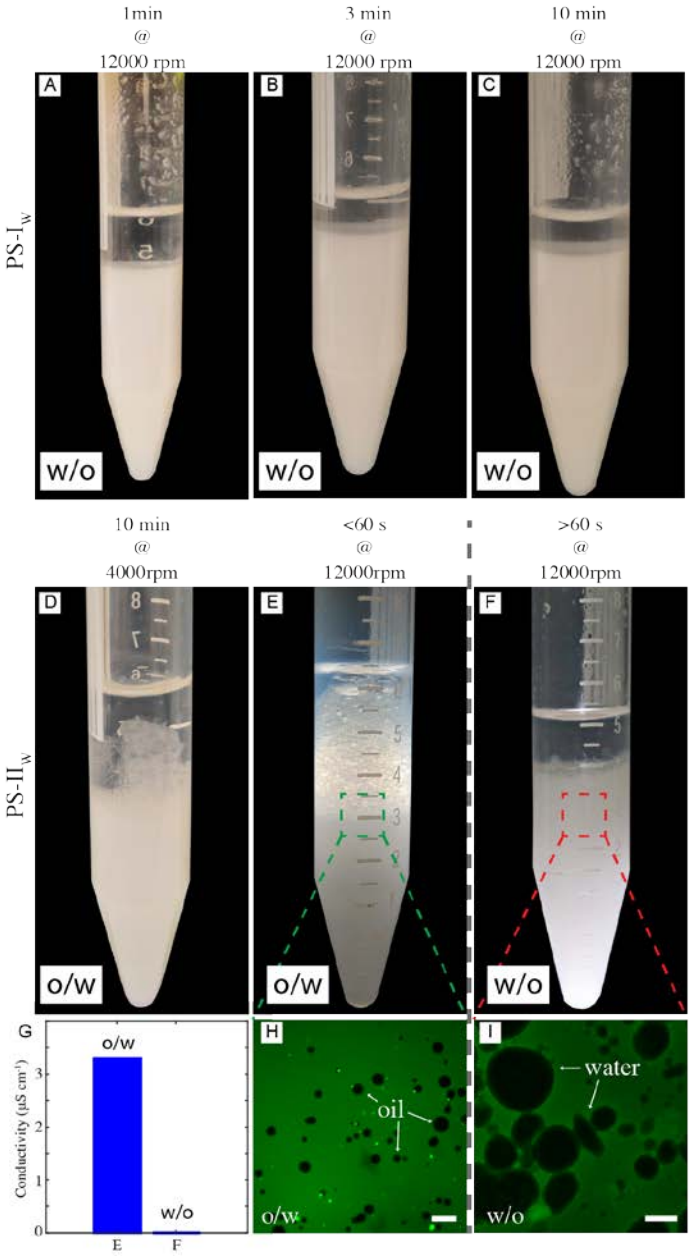

Figure 5 PS-stabilized Pickering emulsions. (A-C) Reference smooth and slightly hydrophobic PS-I_W forms w/o emulsions irrespective of the emulsification time. 3.5 mL aqueous solution at 0.5 wt%, 3.5 mL n-decane. **(D-F)** Mildly hydrophobic and rough PS-II_W (3.5 mL at 0.5 wt%) emulsified with n-decane (3.5 mL) at different shear rates. **(G)** depicts the measured emulsion conductivity. **(H)** and **(I)** are fluorescence optical micrographs of **(E)** and **(F)**, respectively. In **(H),** the emulsion **(E)** is diluted in fluorescently labelled milliQ water; in **(I),** the emulsion **(F)** is diluted in fluorescently labelled n-decane. Scale bars are:**(H)** 20 μm, **(I)** 100 μm.

In order to verify if the inversion scheme can also be followed by particles initially dispersed in the oil phase and to examine in more detail the role of varying roughness, we performed the complementary set of emulsification studies on four batches of bromo-silane functionalized all-silica raspberry-like particles, from the smooth reference SiO2-I to the roughest one SiO2-IV. In particular, only for intermediate roughness, i.e. for SiO2-III particles, it is possible to trigger the mechanical phase inversion of 1:1 water/n-decane emulsions, as shown in Figure 6. In panels A-E, the SiO2-III colloids are initially dispersed in the aqueous phase (see Materials and Methods for details). Conversely, in Figure 6 F-J the same particles are suspended in n-decane. In both cases, the colloids are only transiently stable and sediment upon flocculation overnight. The emulsification studies are done over time scales for which no appreciable aggregation is seen at those particle concentrations.

Upon low-shear emulsification (1 min at 4000 rpm) the rough colloids follow a Bancroft-type behavior and stabilize the phase opposite to which they are initially suspended, i.e. oil droplets if initially dispersed in water (SiO2-III$_W$ – Figure 6A) and water droplets in oil otherwise (SiO2-III$_O$ – Figure 6F). By increasing the emulsification shear rates on the same emulsions (Figure 6 B and G, 1 min at 12000 rpm), a larger amount of dispersed phase can be emulsified but the type of emulsion does not change. The emulsion type is determined by fluorescence imaging in a drop test. The dispersed phase of the emulsion in Figure 6 B results dark when dispersed in excess water containing rhodamine B, indicating that the droplets consist of oil. Vice versa, the dispersed phase of the emulsion in Figure 6 G results dark when dispersed in excess BODIPY 493/503 fluorescently labelled n-decane, indicating the aqueous nature of the droplets. For these particular cases, conductivity measurements were not practicable due to the reduced volumes of the produced emulsions and the large droplet size. When the emulsions are further emulsified at even higher energy upon ultra-sonication (Figure 6 C and H, 3 min tip sonication), we observe a marked change of the emulsions' appearance. This is not only due to a drastic reduction of the droplet size (see Figure 6 E and J, Supplementary Information Figure S10), but for emulsion G, even

more remarkably, the intense emulsification process eventually inverts the nature of the emulsion itself. This first qualitative confirmation of the inversion is given by the fact that in both cases (Figure 6 D and I) creaming is observed overtime. Moreover, the creamed turbid phase was diluted in excess water containing rhodamine B isothiocyanate to perform the drop test. The fact that the water phase appears bright in fluorescence imaging while the droplets are dark, as shown in Figure 6 E and J, indicates that in both cases o/w emulsions are found. This is further corroborated by conductimetry. Emulsions reported in Figure 6 D and I have a conductivity of ~74µScm^{-1} and ~39µScm^{-1}. For reference, milliQ water containing 0.5 wt% of bromo modified SiO_2-III has a conductivity of ~79 µScm^{-1} and the oil phase presents a practically null conductivity, hence the data confirm an aqueous continuous phase These data confirm the previous observations obtained in the complementary experiments with the PS particles and add the fact that if the particles are already initially dispersed in their preferred fluid no inversion is possible and the Bancroft-type emulsion is directly stabilized. The evolution of the droplets size overtime is reported in the Figure S10 in the Supplementary Information.

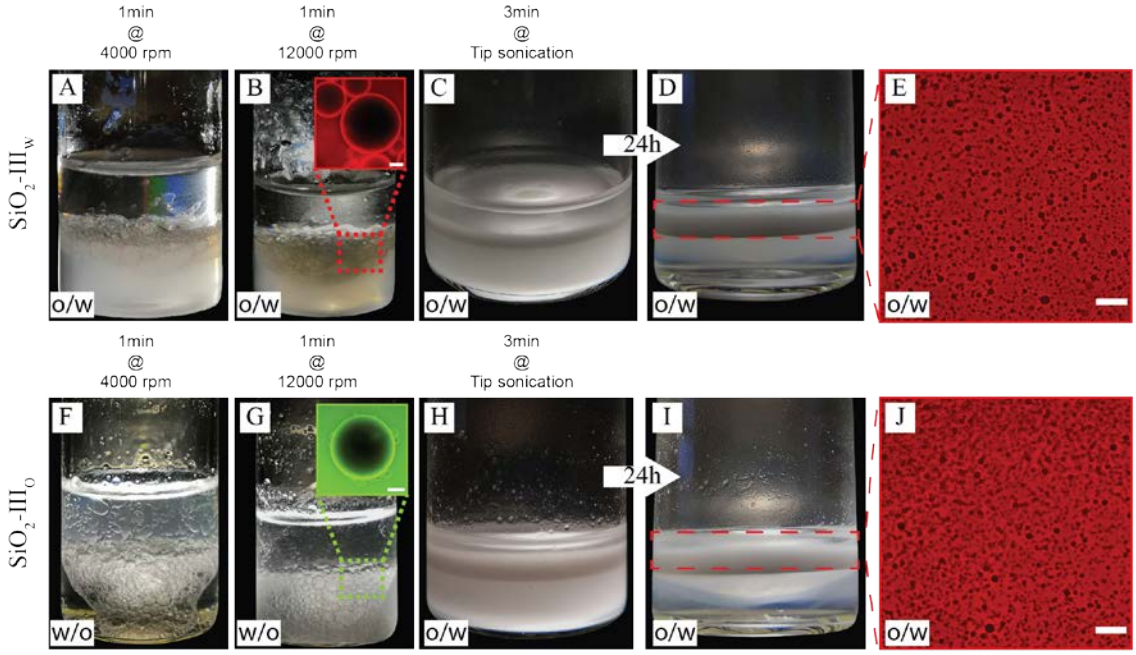

Figure 6 Silica-stabilized Pickering emulsions. Slightly hydrophilic and rough SiO_2-III initially dispersed in both water ($SiO2\text{-}III_W$ **A-D**) and n-decane ($SiO2\text{-}III_O$ **F-I**) emulsified at different times and shear rates. Emulsions **A** and **F** are sheared for 1 min at 4000 rpm. Emulsions **B** and **G** are obtained upon shearing emulsions A and F for 1 min at 12000 rpm. In the inset of **B**, oil droplets are dispersed in excess water containing rhodamine B. In the inset of **G**, water droplets are dispersed in excess n-decane fluorescently labelled with BODIPY 493/503. Scale bar in B: 200 μm; in G:100 μm. Emulsions **C** and **H** are obtained by tip sonicating the emulsions **B** and **G** for 3 min. In **D** and **I**, the tip-sonicated emulsions were left to rest for 24 h. **E** and **J** show fluorescence images of the emulsions displayed in panels **D** and **I**, respectively, after dilution in excess water labeled with rhodamine B. Scale bar 400 μm.

In order to verify which window of experimental parameters allows the phase inversion, we carried out similar experiments with particles of lower and higher roughness compared to SiO2-III. Importantly, the smooth reference particles, after bromo-silanization always stabilize o/w emulsions, irrespective of the phase they are initially dispersed in [32]. Similarly, SiO_2-II are not rough enough to effectively pin the contact line and stabilize the metastable w/o emulsions predicted by looking at the contact angle after spontaneous adsorption reported in Figure 4. When initially dispersed in n-decane, they form o/w emulsions already at low mixing energies (Figure 7A). Conversely, for the same conditions, rougher SiO_2-IV particles form water droplets upon both low- (Figure 7B) and high-energy emulsification (Figure 7C), when initially suspended in n-

decane. In this case, we deduce that the contact line is too strongly pinned to relax via mechanical inputs, even using a tip sonicator. To decrease the activation energy for contact-line relaxation, we lower the interfacial tension using the well-known water-cineole interface (γ = 16.9 mNm^{-1}) [51]. In this way, the pinning energy is reduced by a factor ~ 3, and SiO_2-IV particles suspended in cineole allow the switching of w/o emulsions formed at low shear rates (Figure 7D) to o/w emulsions emulsified at high shear rates (E), following the mechanically induced relaxation of the contact angle. Therefore, the key to obtain the mechanical phase inversion of Pickering emulsions via metastable wetting relies solely on controlling the interplay between particle size, wettability and surface roughness, which, together with the value of the interfacial tension, determine a characteristic energy for contact angle pinning relative to the external energy input. In order to provide further support to our arguments, in the next section we report numerical calculations of the free-energy trajectories of adsorbing rough colloids and compare the calculated metastable minima to simple experimental estimates.

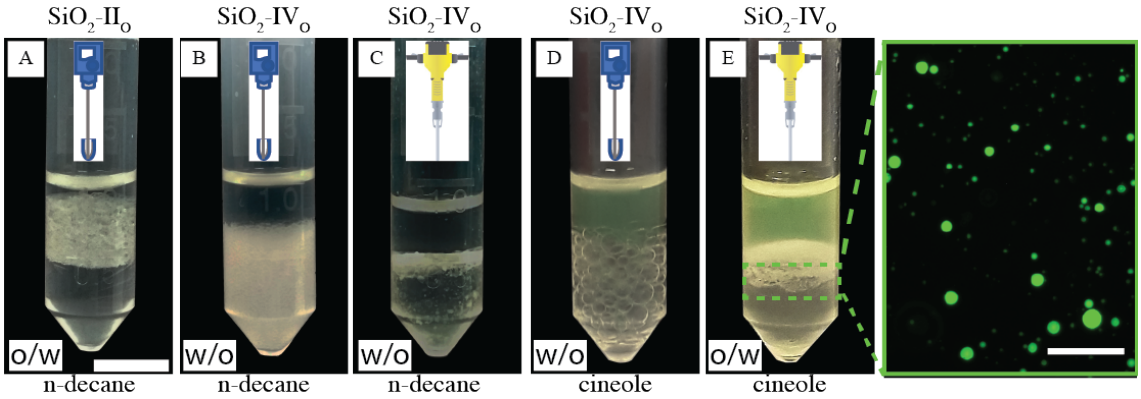

Figure 7 Surface roughness and phase inversion. (A) SiO_2-II (1 wt%) suspended in n-decane emulsified at low input energies already form o/w emulsions**.** SiO_2-IV (1 wt%) suspended in n-decane emulsified at low **(B)** and high input energies **(C)** always form w/o emulsions**.** SiO_2-IV particles initially dispersed in cineole form w/o emulsions at low shear rates **(D)**; the exact same emulsions can be inverted to o/w via tip sonication **(E)**. In the zoomed-in micrograph, the fluorescently labelled cineole forms the dispersed phase. Scale bars: 1 cm and 100 μm for the macroscopic pictures and for the fluorescence micrograph, respectively.

Simulated adsorption kinetics.

In a first set of simulations, we numerically calculate the equilibrium shape of the fluid-fluid interface including the capillary deformations induced by a rough colloidal particle. The interface is represented by a grid of points (see Figure 8 A-C), whereby a simulated-annealing (SA) algorithm is used to calculate the positions of the knots that minimize the thermodynamic potential of the system, hereinafter called energy E [66, 67]. The equilibrium particle height at the fluid-fluid interface is automatically found by this method, while the particle orientation is assumed fixed, for simplicity. The interface snapshots reported in Figure 8 A-C clearly show a corrugated contact line, with surface asperities inducing local deformations, confirming previous observations on larger and rougher silica colloids [32]. In addition, we also employ an adaptation of this numerical method [67] to simulate the quasi-static interfacial adsorption of a colloid with initial position in the fluid with lowest affinity. i.e. mimicking the adsoprtion of silica colloids from n-decane. This quasi-static simulation consists of a sequence of SA simulations in which the equilibrium shape of the fluid-fluid interface is computed with the constraint that the position of each knot cannot explore at a distance greater than Δ from its initial position in each individual SA simulation. Each SA simulation uses as the input interface shape the final shape computed by the previous SA simulation and the energy associated to the final shape of the interface of every SA simulation is calculated. In this way, we effectively sample the free-energy trajectory of a particle as a function of its position relative to the interface during adsorption. Through the various SA simulations, the shape of the interface evolves towards steady-state approximately following the steepest energy gradient path (the smaller the Δ, the better the approximation). More details are reported in the Supplementary Section SI 5 and SI 6 and Figure S12.

Figure 8D reports the quasi-static simulated adsorption kinetics using Δ = 0.05 for a rough colloid of radius *R* = 200 nm and decorated with 75 spherical asperities of radius 25 nm ($\delta \sim 0.76$, RMS ~ 9.7 nm) at a fluid-fluid interface with surface tension of 0.053 Nm^{-1}. The smooth analogue would have an equilibrium contact angle of 70°. The simulated particle therefore resembles the case of a SiO2-II particle adsorbing at a water/n-decane interface from the oil. Remarkably, the proposed

quasi-static approach reveals an exciting scenario for the contact line evolution, which confirms previous measurements indicating both a complex relaxation pathway, where a fast initial dynamics is followed by a slower relaxation [35, 36] and the presence of step-wise wetting relaxation events for rough surfaces [40]. We perform three quasi-static simulations of 500 SA steps each, using three different initial temperatures T_0 ($T_0 \cong 10^4$°C, 10^6°C, and 10^7°C, respectively, with the temperature then decreases linearly to zero throughout $\sim 10^7$ Monte Carlo steps in each SA simulation). In this way, T_0 mimics the energy input level in an adsorption and emulsification process, while the particle surface wettability θ and roughness δ set the height of an energetic barrier for contact line evolution. The trade-off between them determines the adsorption kinetics. Interestingly, the energy E (see Supplementary Section S5, Eq. 2) reported in Figure 8D for the quasi-static simulation with lowest T_0 (cyan line) monotonically decreases until it reaches (after about 50 SA simulations) a metastable configuration, at an energy approximately $0.5 \cdot 10^6$ k_B T (T=room temperature) higher than the equilibrium configuration (red line), and then the particle remains stuck in this metastable configuration for the remaining SA simulations steps. Upon increasing input energy, i.e. T_0 (green line), the particle manages to reach a lower-energy metastable configuration after about 200 SA simulations ($0.15 \cdot 10^6$ k_B T higher than the equilibrium configuration) and then it remains trapped in such metastable configuration for the remaining SA simulations. We clearly see here that the pathway to this final state consists of a sequence of discrete events, where the particle stays trapped in local minima for a number SA steps, before the interface rearranges and moves to the next minimum until the final one is reached. Only in the quasi-static simulation with highest T_0 (blue line) the particle basically reaches the equilibrium position (in about 300 SA steps). The snapshots in Figure 8D represent the particle location relative to the interface in the final minimum and they correspond to effective contact angles of (b) 991, (c) 841 and (d) 731 (very close to the value of 701 for the smooth surface), respectively, starting from an initial position of (a) 1431. The quasi-static simulations therefore confirm that the

relaxation of the contact angle towards its equilibrium value can be triggered to different extents by varying external energy inputs. Small energy inputs can only cause partial relaxations, which are insufficient to invert the particle effective wettability, while higher energies are required for the task. The numerical results thus qualitatively confirm the behavior seen in the experiments. See supplementary videos S3, S4, S5, S6, S7, S8 for an animation (3D tilted and profile views for the three quasi-static simulations) of the interface shape evolution during the particle quasi-static interfacial adsorption.

Remarkably, the pinning of the three-phase contact line is not imposed in the numerical model. Hence, the barriers that block the quasi-static interfacial adsorption of the colloid are not simulation artefacts, as confirmed by the fact that only the quasi-static simulation with highest temperature in the SA simulations reaches the energy minimum. Note that the quasi-static simulation is able to (possibly) overcome energetic barriers since a finite step size Δ is used (in the limit of an exact steepest energy gradient descent, any energetic barrier would block the quasi-static evolution of the system). By looking at the energy fluctuations with respect to the SA temperature (see Fig. S12 in the Supplementary Information), we can estimate that these energy barriers range between $\sim 10^4\ k_B\,T$ and $\sim 0.5 \cdot 10^6\ k_B\,T$. The values are close to the experimental estimations presented in more detail in the Supporting Information Table S5. In particular, we find that mechanical inversion is possible if the energy barrier to move the contact line over the particle equator, and hence cause the effective wettability switch, is below $\sim 1.6 \cdot 10^5\ k_B\,T$. The energy barrier calculated for SiO2-IV_O particles at the water/n-decane interface is $\sim 4.3 \cdot 10^5\ k_B\,T$, but drops down to $\sim 1.4 \cdot 10^5\ k_B\,T$ at the water/cineole interface, supporting the evidence that mechanical inversion is possible in our experiments with the latter fluid combination, but not with the former one.

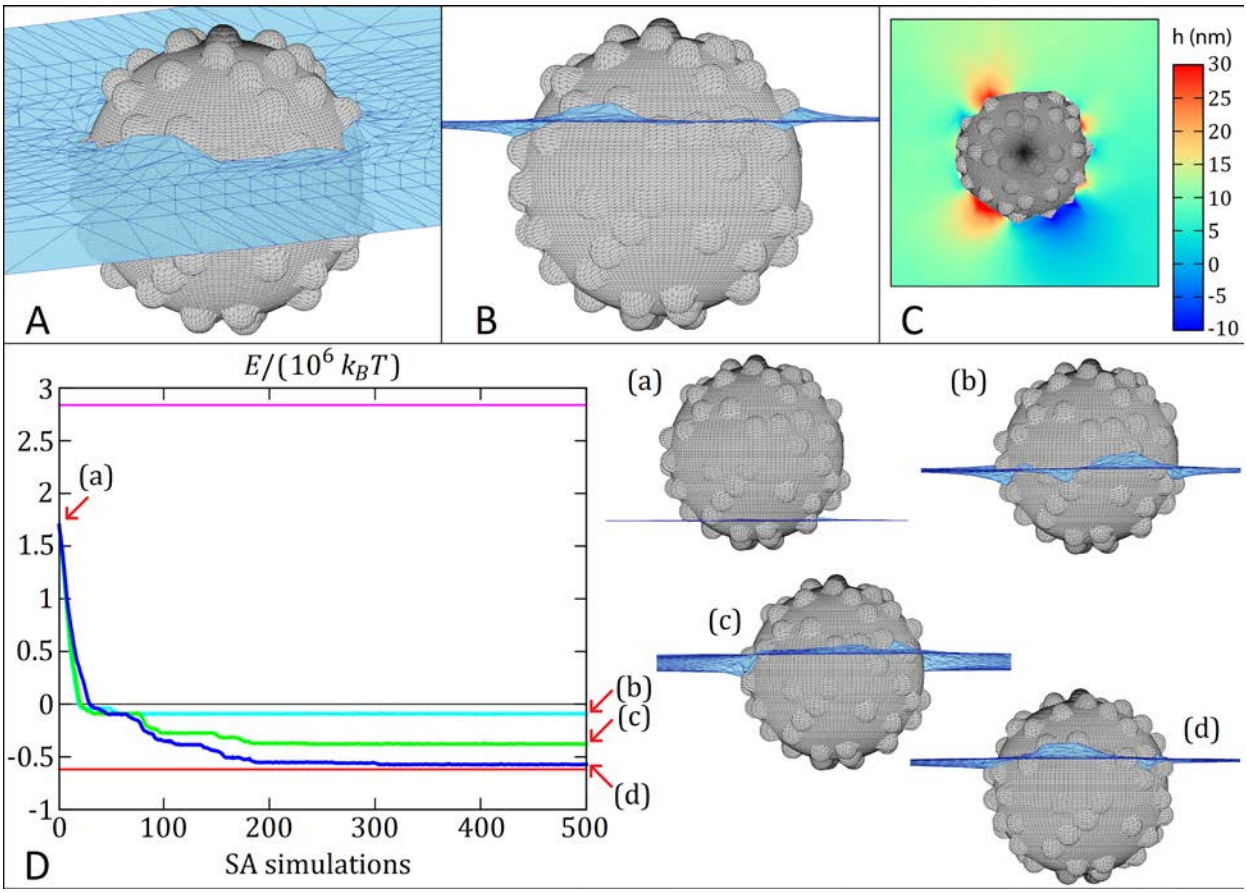

Figure 8 Simulated adsorption kinetics. (A) and **(B)** are, respectively, the 3D tilted and cross-sectional view of the equilibrium shape of the fluid-fluid interface (numerically computed) close to the particle corresponding to the red line in the graph below. The black grid represents the colloid surface, while the blue grid is the fluid-fluid interface. The equilibrium contact angle (measured in the fluid below the interface) is 70° and the fluid-fluid surface tension is 0.053 Nm^{-1}. **(C)** Contour plot of the equilibrium height profile h of the fluid-fluid interface, where h = 0 corresponds to the level of the interface far away from the particle. **(D)** Evolution of the thermodynamic potential E (blue, cyan, green lines) during the quasi-static adsorption of a rough colloid at the interface (using different temperatures T_0 in the SA simulations; cyan: 10^4 °C, green: 10^6 °C, blue: 10^7 °C). Magenta and black lines represent the desorption energy from the liquid with lower and higher affinity, respectively. The red line represents the equilibrium energy as dictated from the surface chemistry. The initial position of the colloid (see a profile view in (a)) is far from the equilibrium configuration shown in (B). The final configuration reached by the rough colloid is either a metastable state or the equilibrium (see profile views in (b), (c), (d)).

Discussion

In this work, we show that by engineering the interplay between particle surface properties, i.e. their wettability and surface roughness, and external energy inputs during emulsification, it is possible to design kinetic pathways that enable the *in-situ* phase inversion of both o/w and w/o emulsions in closed systems using simple mechanical stimuli.

In this respect, an appropriate surface design in terms of particle size, asperity height, shape and number sets the scales of the energy barriers experienced by particles upon interfacial adsorption. These kinetic hurdles can be overcome by appropriate energy inputs during emulsification. The height of the barriers relative to the input energy therefore determines whether (and how far) the contact angle can relax toward equilibrium. Surface asperities can arrest the motion of particles through the interface, so that particle that have chemically hydrophilic (hydrophobic) surfaces adsorbing from the opposite fluid can be effectively hydrophobic (hydrophilic) and hence "unconventionally" stabilize w/o (o/w) emulsions. Upon energy injection and subsequent contact line motion, the same particles can cross the interface, approaching the contact angles defined by their surface chemistry and hence stabilize the "conventional" o/w (w/o) emulsions. The relation between particle wettability and type of stabilized emulsion is often referred to as the Bancroft rule, in analogy to the case of surfactant molecules. Even though the analogy is clear, there are important differences concerning the stabilization mechanisms. For surfactants, the Bancroft rule states that the continuous phase is the one in which the surfactants are soluble, and it has been shown that the stability in this conditions is due to the increased draining time of films of the continuous phase in the presence of excess solubilized surfactants when two droplets approach [68]. As pointed out in the literature [6, 15, 69], the stability of Pickering emulsions is not due to the presence of excess particles in the continuous phase, but rather to the effects of kinetic trapping of single particles at the interface and the creation of steric layers on the droplets' surfaces. In this respect, one associates particle wettability, and hence the emulsion type according to the

Bancroft definition, to the possibility of dispersing the particles in what will become the continuous phase of the emulsion. The strategy that we propose here implies instead that if particles are rough enough, and sufficiently close to neutral wettability, they can be dispersed in the unfavorable liquid, which will become the continuous phase of a long-lived metastable “anti-Bancroft” emulsion and which can be switched in-situ to the stable “Bancroft” emulsion upon injection of sufficient mechanical energy. Cryo images of the Bancroft and long-lived anti-Bancroft emulsions are reported in Supplementary Figure S8 and S9, respectively.

We envision that the findings of this work can offer untapped routes for smart formulations in cosmetics, food and pharmaceutical applications but can also trigger new solutions for selective water- and oil-based purification and recovery processes.

Methods

n-decane (99%, ABCR GmbH) and 1,8-cineole (>98%, TCI) are the oils used for emulsification. Ethanol (absolute, Merck), tetraethyl orthosilicate (TEOS, Sigma-Aldrich), ammonia solution (NH4OH, 25%, Merck), polydiallyldimethylammonium chloride (Poly-DADMAC, 400–500 kDa, 20 wt%, Sigma-Aldrich), silica nanoparticles 39 nm (Klebosol, Clariant, Switzerland), silica nanoparticle 22 nm (Ludox TM; DuPont), hydrogen peroxide (H_2O_2, VWR, 30%), 3-aminopropyl-triethoxysilane (APTES, 97%, ABCR), α-bromoisobutyryl bromide (BrIn, 98%, Aldrich), triethylamine (99%, Sigma-Aldrich) and dichloromethane (anhydrous, 99.8%, Acros Organics), dichloromethane (99.99%, Acros Organics) were used to fabricate and covalently modify the inorganic rough particles. BODIPY 493/503 (Aldrich-Fine Chemicals) and Nile Red (ABCR-Chemicals) were used to trace the apolar phases; Rhodamine B isothiocyanate (Sigma Aldrich) and Alexa Fluor 488 dye (ThermoFisher) were used to trace the aqueous phase. Acrylonitrile (abbreviated AN, Aldrich chemistry ≥ 99.0%), styrene (abbreviated St Sigma Aldrich ≥ 99.0%) and divinylbenzene (abbreviated DVB, Sigma Aldrich) were the monomer used for emulsion polymerization. Water-soluble potassium persulfate (KPS) from Merck (ACS, Reag. Ph. Eur) was

employed as initiator. Potassium poly(ethylene glycol) 4-nonylphenyl 3-sulfopropylether (KPE) and sodium dodecyl sulfate (SDS, Sigma Aldrich ≥ 99%) were used as stabilizers. All materials were used without further purification. Deionized water, deoxygenated by nitrogen stripping, was the reaction medium for all syntheses. The reported particle sizes values have been extracted from the number-based distribution.

Inorganic Particles. The synthesis of inorganic raspberry-like particles has been carried out as follows. Silica nanospheres (berries) were anchored electrostatically onto larger, positively modified silica colloids (cores) [70, 71, 72]. In a typical procedure [24], either homemade Stöber silica particles [73, 74] (0.18wt%, R = 161 nm± 15 nm) or commercially available cores (1.5 wt%, R = 200 nm ± 20 nm, R = 295 nm ± 20 nm, Nanocym) were modified for 30 min in a 0.03 wt% aqueous solution of poly-DADMAC (50 ml) to render their surfaces positively charged. The suspension was then washed three times with milliQ water to remove the unbound excess of polyelectrolyte. Afterwards, the nanoparticle suspension containing the berries was added to the positively modified core colloids (0.45 wt% suspension). 39 nm (6.5 mL, 1 wt%) or 22 nm (88 μL, 48 wt%) silica nanoparticles (berries) were successfully adsorbed onto the surface of the cores during 30 min of vigorous stirring.

In order to tune the surface roughness, a sol-gel route [75] was used to smoothen the raspberry-like particles. A 5 vol% TEOS solution in EtOH was added to a mixture of EtOH/NH_4OH/H2O (77:13:10 volumetric ratio) containing 0.011 wt% of raspberry-like particles at an injection rate of 2 mL per hour while sonicating. The injection of the silica precursor was split into periods of 8 min each, followed by 25 min of equilibration time. The smoothed raspberry-like particles were washed three times with milliQ water.

The smoothing step has the primary effect of tuning the particles' surface roughness and it furthermore strengthens the link between the core and the asperities preventing any possible detachment of the small colloids from the cores, even at high-shear emulsification. The parameters of the syntheses are found in the Table S4.

Covalent surface modification by bromo-silanes. As-produced raspberry-like particles can be surface-activated in a mixture of $H_2O_2/NH_4OH/H_2O$ (volume ratio of 1:1:1, 3.3 wt/vol%) at 70 °C for 10 min. In this way, a uniform layer of silanol groups was created on the particles' surface enhancing the homogeneity and efficiency of the subsequent silanization step. This step is necessary when the IEP of the particles does not coincide with the IEP of native silica. The activated particles were washed by centrifugation/re-dispersion in deionized water and dried under reduced pressure at 60 °C. Afterwards, the particles were stirred overnight in a 2 wt% APTES solution in water. The APTES-modified particles were then washed by repeated centrifugation/re-dispersion cycles in ethanol and dried in a vacuum oven at 60 °C. The amino-functionalisation can be verified by means of a titration curve as reported in Figure S6. The final functionalization was achieved by grafting α-bromoisobutyryl bromide (0.2 ml, 1.6 mM) onto the amino-modified particles (0.9 wt%) by incubation in dry dichloromethane (5 mL) in the presence of triethylamine (0.4 mL). The reaction was carried out under inert atmosphere at room temperature. The suspension was then washed several times in dichloromethane and dried at 60 °C in a vacuum oven. Partially hydrophobized particles bearing bromo-silane groups were re-dispersed in polar and apolar solvents by sonication. The former is simplified by adding MeOH (50 vol%) which is eventually removed upon evaporation at reduced pressure.

Organic Particles. Apart from the case of PS-I_b (discussed in details afterwards), all other organic particles are fabricated via a two-step semibatch emulsion polymerization [28, 29, 76]. In the first step, core particles were nucleated and grown in starved conditions, while feeding the first monomer mixture; afterwards, a further shell was grown onto them by switching to a second feed. The overall synthesis was adjusted according to the desired surface morphology [25], taking advantage from both the sequence of addition and feed compositions. In all cases, SDS was initially used as emulsifier for micellar nucleation and the reactor was evacuated and flushed with nitrogen three

times to avoid radical deactivation by oxygen. When working with AN, the addition of KPE as second surfactant after the particle's nucleation stage improves the colloidal stability.

Smooth Particles. This section is referred to the synthesis of PS-I and PS-I_b, which have been named as smooth particles (S). In the case of PS-I (the procedure presented hereafter refers to an initial 250 g batch, which will have eventually approximately 10% solid content), a mixture of water and surfactant (SDS) was charged into a glass reactor and the temperature set to 70 °C (IC_S in Supplementary Table S1). After the injection of 0.75 g of KPS dissolved in 20 g of water, an emulsion of styrene, DVB, water, and surfactant ($CF1_S$) was fed at a rate of 0.074 mL/min for 1020 minutes by means of a HPLC pump. The slow addition ensures starved polymerization conditions. Meanwhile, a total solution of 95.6 g of water and 1.6 g of KPS was also continuously fed at 0.094 mL/min, to keep the radical concentration constant. The shell monomer solution ($CF2_S$) was fed in the same reactor at a rate of 0.08 mL/min for 180 minutes right after terminating the first step. At the same time, the previous initiator feed was disconnected and 20 g of water containing 0.2 g of KPS were added to keep the reaction running. After the addition of $CF2_S$ was completed, the latex was left running in batch until full conversion was obtained. The evolution of the polymer conversion and particle size was monitored hourly and a full final size characterization was performed via SEM (Supplementary Table S3). This synthesis allows controlling the cross-linking density of the surface but not its surface morphology.

In the case of PS-I_b (the procedure presented hereafter refers to an initial 500 g batch, which will have eventually approximately 15% solid content), a simple starved fed-batch emulsion polymerization protocol was used. Specifically, the initial charge (IC_{Sb}) was added in a glass reactor and heated up. When a temperature of 70 °C was reached, 25 g of water containing 1 g of KPS were injected. Simultaneously, the dosing of the feed ($CF1_{Sb}$) was started (0.2 mL/min for 540 minutes). To preserve starved reaction conditions, additional 50 g of water and 1 g of KPS were injected after 300 minutes. After the injection was completed, the latex was left running in batch for 1h to ensure full conversion. The evolution of the polymer conversion and particle size

was monitored hourly and a full final size characterization was performed via SEM (Supplementary Table S3).

Rough Particles. This section is referred to the syntheses of PS-II, PS-III and PS-IV, which have been named as rough particles (R). In the syntheses, an initial charge (IC_R) composed of water, monomer (100% AN), surfactant (SDS) and initiator (KPS) was injected in the reactor in the mass ratio shown in Supplementary Table2 (the reported procedure presented hereafter refers to a 120 g of total mass, with 10% polymer solid content) and the mixture was heated up to 60 °C. Afterwards, 0.24 g of KPE dissolved in 4 ml of water were added to ensure colloidal stability. The evolution of polymer conversion and particle size was monitored on an hourly base by thermogravimetric analysis (T = 120 °C) using a HG53 Halogen Moisture Analyzer (Mettler Toledo, Switzerland) and by Dynamic Light Scattering (DLS, Malvern Zetasizer Nano Z, United Kingdom). The core particles were used directly as seeds for the shell growth once the conversion reached 90% (roughly after three hours) and without stopping the previous reaction. At that point, 0.18 g of KPS, dissolved in 4 g water, were injected and the second feed of monomer mixture was dispensed for four hours at a flow rate of 0.06 mL/min. Depending on the desired final morphology of the particle, different feed strategies were adopted to switch from the initial IC_R to the composition of the final outer shell (Sty and DVB). In the case of the particles with maximum surface roughness (PS-II in the main manuscript), a feed of water, styrene and DVB (Charged Feed 1, $CF1_R$ in Supplementary Table S2) was directly injected. For particles with a smoother surface, a more gradual change in the feed composition was imposed with the help of two pumps as schematically shown in Figure 2. In particular, the second mixture (Charge Feed 2, $CF2_R$) was dripped into the vessel of the first feed in order to change its composition from $CF1_R$ to $CF2_R$ still keeping constant the total mass fraction of monomers in the feed added to the reactor, as shown in Supplementary Figure S1. According to the desired morphology, 60 or 210 minutes were imposed for particle PS-III and PS-IV, respectively. After the gradient feed, $CF2_R$ was directly connected to the system for the remaining reaction time (i.e., 30 or 180 minutes). In all cases,

after two hours the reaction mixture was further diluted with 20 g water to prevent aggregation. Similarly, to the case of the core, the evolution of particle size and monomer conversion was monitored during the whole shell synthesis. After the end of the second feed, the reaction vessel was left for half an hour at 60 °C to ensure full conversion (above 90%). After cooling, the produced polymer dispersion was filtered by a filter paper (MN 615, 22 s filtration speed) to remove possible polymer lumps. A full, final characterization of the particles size was assessed using SEM image analysis (Supplementary Table S3).

AFM roughness analysis. Convective assembly[777768,65] was used to produce dried particle monolayers. The latter were then scanned in tapping-mode by means of an AFM (JPK Nanowizard3, JPK, Germany) to characterize the particle surface roughness. Imaging was conducted with silicon nitride cantilevers (OMCL-AC160TS, Olympus microcantilevers, Japan) having a spring constant of about 40 N m^{-1} and a resonance frequency of about 300 kHz in air under ambient conditions. Additional details of the AFM roughness analysis and used operators can be found in Supplementary Section 5 and in Supplementary Figure S4.

Freeze-fracture shadow-casting (FreSCa) cryo-SEM. Sample for the FreSCa cryo-SEM measurements was prepared following the standard procedure [62, 63].

For the experiments where the particles adsorbed from water, 0.5 μL of the aqueous particle suspensions were injected in a homemade, hydrophilized copper holder, covered by 3.5 μL of purified n-decane (surface tension γ=52 mNm^{-1}). When the particles were adsorbed from the oil phase, 0.5 μL of milliQ water were injected in the hydrophilic copper holder and subsequently covered by 3.5 μL of oil suspension. All samples were shock-frozen with liquid propane jets (Bal-Tec/Leica JFD 030, Balzers/Vienna) maximally 1 min after the interface was created. Frozen samples were fractured in high-vacuum conditions (10^{-6} mbar) and cryogenic temperatures (- 120 °C) in a freeze-etching device (Bal-Tec/Leica BAF060 device). Fractured samples were freeze-dried for 1 min at -100 °C and coated with 3 nm tungsten at a deposition angle of 30° followed by

additional 3 nm tungsten at continuously varying angles between 30° and 90°. In this way, particles protruding through the interface with a contact angle greater than 30°can cast a shadow. The freeze-fractured, metal-coated samples were then transferred in a pre-cooled SEM (-120 °C) (Zeiss Gemini 1530, Oberkochen) for imaging. Single-particle contact angles can be reliably measured only for particles casting a shadow. The results reported in Figure 4 of the main manuscript are the averages and standard deviation of the contact angle distributions typically measured over roughly 100 particles. No sample delamination was observed during freeze-fracture.

Emulsion preparation. Organic rough colloids were treated with an ion exchange resin (Dowex® MarathonTM C) to remove the excess of surfactant. Effective removal was checked by measuring the surface tension of the suspension with a Wilhelmy plate using DCAT 21 (Dataphysics, Filderstadt, Germany) at a particle concentration of 0.5 wt.% (25°C). The suspension was further used only if its interfacial tension was close to the value of pristine water-air interface (71.97 mNm^{-1} at 25 °C). Additionally, the suspensions were washed several times by centrifugation for 8 min at 25000 rpm (Beckman Coulter, JA 25.5) followed by supernatant removal and redispersion in MilliQ water to remove further impurities.

The bromo-silanized inorganic rough particles were dried and re-dispersed via intense ultra-sonication. The redispersion of the dry bromo-functionalized colloids in water is facilitated using using methanol (50 vol%) which is subsequentially removed upon evaporation at reduced pressure. The oil-soluble fluorescent dyes BODIPY 493/503 (Aldrich-Fine Chemicals) or Nile Red (ABCR-Chemicals) were used to improve the contrast in the optical images and to visualize directly the type of emulsion in a fluorescence microscope. Fluorescence images were acquired with either an Axio Observer D1 (Axioscope, Zeiss, Germany) or a Nikon Ti-E inverted microscope equipped with a Hamamatsu ORCA Flash camera after placing a small amount of the emulsion between two glass coverslips.

Emulsions of equal volumes of water and oil (either 500 μL, 750 μL or 3.5 mL) were prepared at low and high input energies. The former are obtained either by either T10 ULTRA-TURRAX (8 mm head, IKA, Germany) or T25 ULTRA-TURRAX (10 mm head, IKA, Germany). The latter are instead prepared by ultra-sonication (UP 200 S Ultraschallprozessor (tip diameter 7 mm) for 1 min; Bandelin Sonorex RK 31, Ultraschallbad, for either 3 or 10 min; Qsonica sonicators, Q500). All emulsification tests were repeated at least three times. The same particle batches were used for the wetting and emulsification studies.

Characterization. Dynamic light scattering was performed with a Malvern Nano ZS (Malvern Instrument, UK) instrument at ambient temperature. Standard and cryo-SEM images were captured with a Zeiss Gemini 1530 (Zeiss, Oberkochen). The latter at -120°C, with microscope operating in cryo mode.

The BET (Brunauer-Emmer-Teller) surface areas resulted from N_2-adsorption at 77 K and measured with ASAP 2060 (Micromeritics, Norcross, USA) using approximately 50 mg of sample (p/p0 range used: 0.05-0.25). The surface morphology was investigated by scanning individual colloids in tapping mode within a dried monolayer by means of an AFM (JPK Nanowizard3, JPK, Germany).

ASSOCIATED CONTENT

Supporting Information. Further details about the particles' synthesis, their size distribution and wetting are reported. The effect of the composition and the morphology on the wetting of organic colloids is discussed. Additional experiments regarding the solid-content-dependent emulsification process, cryo-SEM on different emulsions and observations over the emulsion stability are reported. Further details on the simulated adsorption are described.

AUTHOR INFORMATION

Corresponding Author

* E-mail: lucio.isa@mat.ethz.ch

ORCID:

Lucio Isa:

Author Contributions

L.I., M.Z. and A.C designed and led the study. M.Z. and C-P.H. synthesized and characterized the inorganic particles. M.Z., C-P.H. and M-A.F-R carried out the emulsification and wetting studies A.C., A.B., S.C., D.M. and G.St. synthesized and characterized the organic particles. G.So. performed the numerical calculations. L.I, M.Z. and A.C wrote the manuscript with contributions from all authors. All authors have given approval to the final version of the manuscript. ‡These authors contributed equally.

Competing interests

The authors declare no competing financial interest.

ACKNOWLEDGMENTS

We acknowledge Svetoslav Anachkov and Claudio Colombo for helpful discussions, Nicholas D. Spencer and André Studart for access to instrumentation. L.I., M.Z. and M-A.F-R. acknowledge the financial support from the Swiss National Science Foundation grants P00P2_144646/1 and PP00P2_172913/1. C-P.H. acknowledges financial support from the ETH Research Grant ETH -4916-1. M.Z. acknowledges the financial support from the Swiss National Science Foundation grant P2EZP2_178502. The freeze-fracture cryo-SEM measurements has been carried out at the Scientific Center for Optical and Electron Microscopy (ScopeM) of ETH Zurich.

REFERENCES

1. Dickinson E. Food emulsions and foams: stabilization by particles. *Curr Opin Colloid In* **15**, 40-49 (2010).

2. Qi L, *et al.* Segregation of Amphiphilic Polymer-Coated Nanoparticles to Bicontinuous Oil/Water Microemulsion Phases. *Energ Fuel* **31**, 1339-1346 (2017).

3. Yoon KY, Son HA, Choi SK, Kim JW, Sung WM, Kim HT. Core Flooding of Complex Nanoscale Colloidal Dispersions for Enhanced Oil Recovery by in Situ Formation of Stable Oil-in-Water Pickering Emulsions. *Energ Fuel* **30**, 2628-2635 (2016).

4. Ramsden W. Separation of Solids in the Surface-Layers of Solutions and 'Suspensions' (Observations on Surface-Membranes, Bubbles, Emulsions, and Mechanical Coagulation). -- Preliminary Account. *P R Soc London* **72**, 156-164 (1903).

5. Pickering SU. CXCVI.-Emulsions. *J Chem Soc T* **91**, 2001-2021 (1907).

6. Pieranski P. Two-Dimensional Interfacial Colloidal Crystals. *Phys Rev Lett* **45**, 569-572 (1980).

7. Binks BP, Lumsdon SO. Influence of Particle Wettability on the Type and Stability of Surfactant-Free Emulsions. *Langmuir* **16**, 8622-8631 (2000).

8. Aveyard R, Binks BP, Clint JH. Emulsions stabilised solely by colloidal particles. *Adv Colloid Interfac* **100–102**, 503-546 (2003).

9. Binks BP. Particles as surfactants—similarities and differences. *Curr Opin Colloid In* **7**, 21-41 (2002).

10. Vignati E, Piazza R, Lockhart TP. Pickering emulsions: Interfacial tension, colloidal layer morphology, and trapped-particle motion. *Langmuir* **19**, 6650-6656 (2003).

11. Gonzenbach UT, Studart AR, Tervoort E, Gauckler LJ. Ultrastable Particle-Stabilized Foams. *Angew Chem Int Edit* **45**, 3526-3530 (2006).

12. Beltramo PJ, *et al.* Arresting dissolution by interfacial rheology design. *Proc Natl Acad Sci USA* **114**, 10373-10378 (2017).

13. Maestro A, Guzmán E, Ortega F, Rubio RG. Contact angle of micro- and nanoparticles at fluid interfaces. *Curr Opin Colloid In* **19**, 355-367 (2014).

14. Binks BP, Isa L, Tyowua AT. Direct Measurement of Contact Angles of Silica Particles in Relation to Double Inversion of Pickering Emulsions. *Langmuir* **29**, 4923-4927 (2013).

15. Kralchevsky PA, Ivanov IB, Ananthapadmanabhan KP, Lips A. On the Thermodynamics of Particle-Stabilized Emulsions: Curvature Effects and Catastrophic Phase Inversion. *Langmuir* **21**, 50-63 (2005).

16. Wu D, Chew JW, Honciuc A. Polarity Reversal in Homologous Series of Surfactant-Free Janus Nanoparticles: Toward the Next Generation of Amphiphiles. *Langmuir* **32**, 6376-6386 (2016).

17. Zanini M, Isa L. Particle contact angles at fluid interfaces: pushing the boundary beyond hard uniform spherical colloids. *J Phys Condens Mat* **28**, 313002 (2016).

18. Bianchi E, Blaak R, Likos CN. Patchy colloids: state of the art and perspectives. *Phys Chem Chem Phys* **13**, 6397-6410 (2011).

19. Galati E, *et al.* Shape-Specific Patterning of Polymer-Functionalized Nanoparticles. *ACS Nano* **11**, 4995-5002 (2017).

20. Gong Z, Hueckel T, Yi G-R, Sacanna S. Patchy particles made by colloidal fusion. *Nature* **550**, 234 (2017).

21. Sacanna S, *et al.* Shaping colloids for self-assembly. *Nat Commun* **4**, 1688 (2013).

22. Sacanna S, Pine DJ, Yi G-R. Engineering shape: the novel geometries of colloidal self-assembly. *Soft Matter* **9**, 8096-8106 (2013).

23. Such GK, Johnston APR, Liang K, Caruso F. Synthesis and functionalization of nanoengineered materials using click chemistry. *ProgPolym Sci* **37**, 985-1003 (2012).

24. Zanini M, Hsu C-P, Magrini T, Marini E, Isa L. Fabrication of rough colloids by heteroaggregation. *Colloid Surface A* **532**, 116-124 (2017).

25. Okubo M. Control of particle morphology in emulsion polymerization. *Makromol Chem-M Symp* **35-36**, 307-325 (1990).

26. Yi‐Cherng C, Victoria D, S. EAM. Interfacial phenomena controlling particle morphology of composite latexes. *J Appl Polym Sci* **42**, 1049-1063 (1991).

27. Kang C, Honciuc A. Influence of Geometries on the Assembly of Snowman-Shaped Janus Nanoparticles. *ACS Nano* **12**, 3741-3750 (2018).

28. Cingolani A, Cuccato D, Storti G, Morbidelli M. Control of Pore Structure in Polymeric Monoliths Prepared from Colloidal Dispersions. *Macromol Mater Eng* **303**, 1700417 (2018).

29. Landier C, Barandiaran MJ, Drujon X, Asua JM. Synthesis of Core/Shell Latexes in a Continuous Stirred Tank Reactor. *Ind Eng Chem Res* **43**, 700-707 (2004).

30. San-Miguel A, Behrens SH. Influence of Nanoscale Particle Roughness on the Stability of Pickering Emulsions. *Langmuir* **28**, 12038-12043 (2012).

31. Mable CJ, Warren NJ, Thompson KL, Mykhaylyk OO, Armes SP. Framboidal ABC triblock copolymer vesicles: a new class of efficient Pickering emulsifier. *Chem Sci* **6**, 6179-6188 (2015).

32. Zanini M, Marschelke C, Anachkov SE, Marini E, Synytska A, Isa L. Universal emulsion stabilization from the arrested adsorption of rough particles at liquid-liquid interfaces. *Nat Commun* **8**, 15701 (2017).

33. Stocco A, Nobili M. A comparison between liquid drops and solid particles in partial wetting. *Adv Colloid Interfac*, (2017).

34. Binks BP, Rodrigues JA. Types of Phase Inversion of Silica Particle Stabilized Emulsions Containing Triglyceride Oil. *Langmuir* **19**, 4905-4912 (2003).

35. Kaz DM, McGorty R, Mani M, Brenner MP, Manoharan VN. Physical ageing of the contact line on colloidal particles at liquid interfaces. *Nat Mater* **11**, 138-142 (2012).

36. Wang A, McGorty R, Kaz DM, Manoharan VN. Contact-line pinning controls how quickly colloidal particles equilibrate with liquid interfaces. *Soft Matter* **12**, 8958-8967 (2016).

37. Wang A, Rogers WB, Manoharan VN. Effects of Contact-Line Pinning on the Adsorption of Nonspherical Colloids at Liquid Interfaces. *Phys Rev Lett* **119**, 108004 (2017).

38. Colosqui CE, Morris JF, Koplik J. Colloidal Adsorption at Fluid Interfaces: Regime Crossover from Fast Relaxation to Physical Aging. *Phys Rev Lett* **111**, 028302 (2013).

39. Rahmani AM, Wang A, Manoharan VN, Colosqui CE. Colloidal particle adsorption at liquid interfaces: capillary driven dynamics and thermally activated kinetics. *Soft Matter* **12**, 6365-6372 (2016).

40. Zanini M, *et al.* Detachment of Rough Colloids from Liquid–Liquid Interfaces. *Langmuir* **34**, 4861-4873 (2018).

41. Binks BP, Lumsdon SO. Catastrophic Phase Inversion of Water-in-Oil Emulsions Stabilized by Hydrophobic Silica. *Langmuir* **16**, 2539-2547 (2000).

42. Binks BP, Lumsdon SO. Transitional Phase Inversion of Solid-Stabilized Emulsions Using Particle Mixtures. *Langmuir* **16**, 3748-3756 (2000).

43. Binks BP, Murakami R, Armes SP, Fujii S. Temperature-Induced Inversion of Nanoparticle-Stabilized Emulsions. *Angew Chem* **117**, 4873-4876 (2005).

44. Binks BP, Rodrigues JA. Double Inversion of Emulsions By Using Nanoparticles and a Di‐Chain Surfactant. *Angew Chem Int Edit* **46**, 5389-5392 (2007).

45. Binks BP, Rodrigues JA. Inversion of Emulsions Stabilized Solely by Ionizable Nanoparticles. *Angew Chem* **117**, 445-448 (2005).

46. Read ES, Fujii S, Amalvy JI, Randall DP, Armes SP. Effect of Varying the Oil Phase on the Behavior of pH-Responsive Latex-Based Emulsifiers: Demulsification versus Transitional Phase Inversion. *Langmuir* **20**, 7422-7429 (2004).

47. Fujii S, Randall DP, Armes SP. Synthesis of Polystyrene/Poly[2-(Dimethylamino)ethyl Methacrylate-stat-Ethylene Glycol Dimethacrylate] Core−Shell Latex Particles by Seeded Emulsion Polymerization and Their Application as Stimulus-Responsive Particulate Emulsifiers for Oil-in-Water Emulsions. *Langmuir* **20**, 11329-11335 (2004).

48. Sun G, Li Z, Ngai T. Inversion of Particle‐Stabilized Emulsions to Form High‐Internal‐Phase Emulsions. *Angew Chem Int Edit* **49**, 2163-2166 (2010).

49. White KA, Schofield AB, Wormald P, Tavacoli JW, Binks BP, Clegg PS. Inversion of particle-stabilized emulsions of partially miscible liquids by mild drying of modified silica particles. *J Colloid Interface Sci* **359**, 126-135 (2011).

50. Herzig EM, White KA, Schofield AB, Poon WCK, Clegg PS. Bicontinuous emulsions stabilized solely by colloidal particles. *Nat Mater* **6**, 966-971 (2007).

51. Binks BP, Lumsdon SO. Effects of oil type and aqueous phase composition on oil-water mixtures containing particles of intermediate hydrophobicity. *Phys Chem Chem Phys* **2**, 2959-2967 (2000).

52. Binks BP, Murakami R. Phase inversion of particle-stabilized materials from foams to dry water. *Nat Mater* **5**, 865 (2006).

53. Binks BP, Philip J, Rodrigues JA. Inversion of Silica-Stabilized Emulsions Induced by Particle Concentration. *Langmuir* **21**, 3296-3302 (2005).

54. Binks BP, Fletcher PDI, Holt BL, Beaussoubre P, Wong K. Phase inversion of particle-stabilised perfume oil-water emulsions: experiment and theory. *Phys Chem Chem Phys* **12**, 11954-11966 (2010).

55. Thickett SC, Gilbert RG. Emulsion polymerization: State of the art in kinetics and mechanisms. *Polymer* **48**, 6965-6991 (2007).

56. Mitrano DM, Beltzung A, Frehland S, Schmiedgruber M, Cingolani A, Schmidt F. Synthesis of metal-doped nanoplastics and their utility to investigate fate and behaviour in complex environmental systems. *Nature Nanotechnology*, (2019).

57. Tang C, Zhang C, Liu J, Qu X, Li J, Yang Z. Large Scale Synthesis of Janus Submicrometer Sized Colloids by Seeded Emulsion Polymerization. *Macromolecules* **43**, 5114-5120 (2010).

58. Odian G. *Principles of Polymerization*, 4th edn. Wiley, J., Ed (2004).

59. Ouadahi K, Allard E, Oberleitner B, Larpent C. Synthesis of azide-functionalized nanoparticles by microemulsion polymerization and surface modification by click chemistry in aqueous medium. *J Polym Sci A1* **50**, 314-328 (2012).

60. Kirillova A, Marschelke C, Friedrichs J, Werner C, Synytska A. Hybrid Hairy Janus Particles as Building Blocks for Antibiofouling Surfaces. *ACS Appl Mater Inter* **8**, 32591-32603 (2016).

61. Ye M, *et al.* Superamphiphobic Particles: How Small Can We Go? *Phys Rev Lett* **112**, 016101 (2014).

62. Isa L, Lucas F, Wepf R, Reimhult E. Measuring single-nanoparticle wetting properties by freeze-fracture shadow-casting cryo-scanning electron microscopy. *Nat Commun* **2**, 438 (2011).

63. Isa L. Freeze-fracture Shadow-casting (FreSCa) Cryo-SEM as a Tool to Investigate the Wetting of Micro- and Nanoparticles at Liquid–Liquid Interfaces. *Chimia* **67**, 231-235 (2013).

64. Golemanov K, Tcholakova S, Kralchevsky PA, Ananthapadmanabhan KP, Lips A. Latex-Particle-Stabilized Emulsions of Anti-Bancroft Type. *Langmuir* **22**, 4968-4977 (2006).

65. Madivala B, Vandebril S, Fransaer J, Vermant J. Exploiting particle shape in solid stabilized emulsions. *Soft Matter* **5**, 1717-1727 (2009).

66. Soligno G, Dijkstra M, van Roij R. Self-Assembly of Cubes into 2D Hexagonal and Honeycomb Lattices by Hexapolar Capillary Interactions. *Phys Rev Lett* **116**, 258001 (2016).

67. Soligno G, Dijkstra M, Roij Rv. The equilibrium shape of fluid-fluid interfaces: Derivation and a new numerical method for Young's and Young-Laplace equations. *J Chem Phys* **141**, 244702 (2014).

68. Traykov T, Ivanov I. Hydrodynamics of thin liquid films. Effect of surfactants on the velocity of thinning of emulsion films. *International Journal of Multiphase Flow* **3**, 471-483 (1977).

69. Binks BP, Horozov TS. *Colloidal particles at liquid interface*. Cambridge University Press (2006).

70. Kamp M, *et al.* Selective Depletion Interactions in Mixtures of Rough and Smooth Silica Spheres. *Langmuir* **32**, 1233-1240 (2016).

71. Furusawa K, Anzai C. Preparation of composite fine particles by heterocoagulation. *Colloid Polym Sci* **265**, 882-888 (1987).

72. Harley S, Thompson DW, Vincent B. The adsorption of small particles onto larger particles of opposite charge Direct electron microscope studies. *Colloid Surface* **62**, 163-176 (1992).

73. Stöber W, Fink A, Bohn E. Controlled growth of monodisperse silica spheres in the micron size range. *J Colloid Interface Sci* **26**, 62-69 (1968).

74. Bogush GH, Tracy MA, Zukoski CF. Preparation of monodisperse silica particles: Control of size and mass fraction. *J Non-Cryst Solids* **104**, 95-106 (1988).

75. Graf C, Vossen DLJ, Imhof A, van Blaaderen A. A General Method To Coat Colloidal Particles with Silica. *Langmuir* **19**, 6693-6700 (2003).

76. Evans CE, Lovell PA. Click chemistry as a route to surface functionalization of polymer particles dispersed in aqueous media. *Chem Commun*, 2305-2307 (2009).

77. Denkov N, Velev O, Kralchevski P, Ivanov I, Yoshimura H, Nagayama K. Mechanism of formation of two-dimensional crystals from latex particles on substrates. *Langmuir* **8**, 3183-3190 (1992).